Available online at www.sciencedirect.com
SCIENCE DIRECT®
International Journal of Heat and Mass Transfer 48 (2005) 4229–4242
International Journal of HEAT and MASS TRANSFER
www.elsevier.com/locate/ijhmt

Numerical simulation of virus diffusion in facemask during breathing cycles

Li Yi, Li Fengzhi *, Zhu Qingyong

Institute of Textiles and Clothing, The Hong Kong Polytechnic University, Hung Hom, Kowloon, Hong Kong

Received 29 March 2004

Abstract

The recent SARS outbreak has spawned a major controversy concerning the protective performance of facemasks. The objective of this paper is to establish a mathematical model for describing the mechanism of viruses diffusion in a facemask during breathing cycles. In this model the mechanisms of the water vapor molecular diffusion, evaporation/condensation, sorption/desorption of moisture by fibers, Brownian diffusion of the virus, filtration of virus, capillary penetration of the viruses with the liquid water and latent heat generation due to phase change are considered. Meanwhile, the theoretical predictions are compared with experimental data, and good agreement is observed between the two, indicating that the model is satisfactory. Also, the effects of structural and materials properties on virus transfer are investigated.

Keywords: Virus transfer; Mask; Filtration; Breathing cycles

1. Introduction

Since the breakout of SARS, the infection rate of front-line healthcare workers was very high. Even though they were equipped in the later stage with the best protective devices available on the market, a number of healthcare workers were still reported infected [1]. WHO announced that the primary route of SARS infection is thought to be via droplets through the mouth, nose and eyes. Therefore, it is critical to develop sound scientific understanding on how viruses can penetrate facemasks and infect the wearer during breathing.

Chen et al. [2] reported a study on the evaluation of single-use masks and respirators for protection of health care workers against mycobacterial aerosols by measuring the filtration efficiencies of a sub-micron surgical mask and three different types of respirators. They found that mean efficiencies were 97% for the surgical mask and a dusk/mist respirator, and more than 99.9% for the high-efficiency particulate air respirator. Willekem et al. [3] investigated bacterial penetration of different bacterial shapes, aerodynamic sizes, and flow rates through a surgical mask and a dust/mist respirator. The authors found that the spherical corn oil particles and spherical bacteria have the same penetration in size range from 0.9 to 1.7 μm, while rod-shaped bacteria penetrate less, depending on the aspect ratio of bacteria. Qian et al. [4] further studied the penetration efficiency of N95 respirators for airborne microbial and inert

* Corresponding author. Tel.: +852 2766 6509; fax: +852 2773 1432.
E-mail address: tclifz@polyu.edu.hk (L. Fengzhi).

0017-9310/$ - see front matter © 2005 Elsevier Ltd. All rights reserved.
doi:10.1016/j.ijheatmasstransfer.2005.03.030

Nomenclature

c	experiment constant
$(c_v)_m$	volumetric heat capacity of the fabric (J/m^3)
C_a	water vapor concentration in the air filling the inter-fiber void spaces of the fabric (kg/m^3)
$C_a^*(T)$	saturated water vapor concentration (kg/m^3)
C_{ab}	ambient water vapor concentration (kg/m^3)
C_f	water vapor concentration in the fibers of the fabric (kg/m^3)
C_s	gas concentration in the air filling the inter-fiber void spaces of the fabric (kg/m^3)
C_v	virus concentration in the liquid water of the fabric (kg/m^3)
d_c	effective radius of pore in fabrics (m)
D_B	Brownian diffusivity (m^2/s)
$D_f(w_c, t)$	diffusion coefficient of water vapor in the fibers (m^2/s)
D_M	molecular diffusivity (m^2/s)
h_c	convection mass transfer coefficient (m/s)
$h_{l\leftrightarrow g}$	mass transfer coefficient (m/s)
h_t	combined heat transfer coefficient (J/m^2 K)
k_{mix}	thermal conductivity of the fabric (W/m K)
K	intrinsic permeability (m^2)
K_{rl}	relative permeability of liquid water
K_{rs}	relative permeability of gas
L	thickness of fabric (m)
M_s	mole mass of gas (kg/mol)
p_c	capillary pressure (kg/m s^2)
p_s	pressure of gas phase (kg/m s^2)
Q_l	evaporation rate of liquid water (kg/m^3 s)
r	radius (m)
R	gas constant (J/mol K)
S_v	specific area of the fabric (1/m)
t	time (s)
T	temperature of the fabric (K)
V_l	intrinsical velocity of liquid water (m/s)
V_s	intrinsical velocity of gas (m/s)
x	X-coordinate

Greek symbols

ρ_l	density of liquid water (kg/m^3)
ρ_v	density of virus (kg/m^3)
ε	porosity of fabric
ε_f	volume fraction of fibers
ε_l	volume fraction of liquid water
ε_s	volume fraction of gas
ε_v	volume fraction of virus in deposition
λ	heat of sorption or water or vapor by fibers (J/kg)
λ_l	heat of sorption or desorption of liquid water by fibers (J/kg)
λ_v	heat of sorption or desorption of water vapor by fibers (J/kg)
ϕ	contact angle (°)
σ	surface tension (N/m)
β	average angle of the capillaries in fabrics (°)
μ_l	dynamic viscosity of water (kg/(ms))
μ_s	dynamic viscosity of gas (kg/(ms))

Superscripts

n	previous time
$n+1$	present time

Subscript

0	initial value

particles. Using laboratory tests with NaCl certification aerosols and measurements with particle-size spectrometers, N95 respirators were found to have higher filtration efficiency than DM and DFM respirators and non-certified surgical masks. The authors concluded that N95 respirators provide excellent protection against airborne particles when there is good face seal.

These findings provide good scientific evidences and guidelines for practical usages in terms of penetration efficiency. However, it is questionable whether filtration alone is able to provide enough protection against viruses. For instance, Qian et al. [4] found that N95 respirators made by different companies have different filtration efficiencies for the most penetrating particle size (0.1–0.3 μm), above which the filtration efficiency increases with size and reaches 99.5% or higher at about 0.75 μm.

When the droplets contaminated with viruses reach a surface such as that on a mask, they can stick to the mask if its outer surface is not strongly water repellent or be absorbed by the mask if its surface is water absorbent. A N95 mask that can filter out particles down to 0.3 μm can obviously filter out droplets greater in size. However, SARS corona viruses are irregularly shaped and are about 60–120 nm in diameter. Therefore, viruses may be able to penetrate or spread through the mask in the form of liquid diffusion by a capillary effect, particularly since the expired air will most likely wet the mask. The high moisture content and high temperature in the expired air can cause water vapor to condense in the mask due to the temperature difference between the air and the mask. The droplets that are expelled when speaking will accelerate the wetting process. The action of breathing will mechanically reinforce the penetration.

During repeated breathing actions, a mask also becomes a collector of viruses, particularly when its outer surface is exposed to contaminated droplets. This process is a typical physical process of coupled heat and mass transfer in porous materials such as non-woven textile materials. As viruses and bacteria can stay on the surface and in the masks for significantly long time period during wear, it is obviously dangerous and undesirable if they can live comfortably and stay active in the warm and humid microenvironment in the masks. In order to avoid these phenomena, it is necessary to study the transfer mechanisms of the virus or bacteria in the mask and to supervise the design and usage of the mask according to these mechanisms.

Heat and mass transfer in porous textiles is a complicated process involving simultaneous coupled multi-field change. There are many references for utilized mathematical model to describe the heat and mass transfer mechanisms in porous media. Ogniewicz and Tien [5] reported an analysis with assumption that heat is transported by conduction and convection, the condensate is in pendular state. Motakef and El-Masri [6] and Shapiro and Motakef [7] extended the analysis to consider mobile condensates. More recently, heat and mass transfer in wet porous media in presence of evaporation–condensation was recently revisited analytically by Bouddour et al. [8] using the homogenization method of asymptotic for periodic structure. The inertia effects and boundary on flow and heat transfer in porous media were investigated by Vafai and Tien [9]. They discovered the Darcy model is not valid at high flow velocity. Amiri and Vafai [10] studied the dispersion effects of forced convection on heat transfer. In these studies, the researchers focused mainly on materials that do not absorb moisture vapor.

For textile materials, the majority of textile fibers have a certain degree of moisture absorption capability (called hygroscopicity). The moisture absorption influences the heat and moisture transfer processes. In order to describe the simultaneous heat and moisture transfer in porous textiles Li and Holcombe [11] introduced a new two-stage absorption model to better describe the coupled heat and moisture transport in fabrics. Li and Luo [12] improved the sorption rate equation by assuming that the moisture sorption by a wool fiber can be generally described as a uniform-diffusion equation for both stages of sorption. Luo et al. [13] presented a dynamic model of heat and moisture transfer with sorption and condensation in porous clothing assemblies. Their model considers the effect of water content in the porous fibrous batting on the effective thermal conductivity as well as radiative heat transfer. But the above-mentioned models ignored the effect of liquid water movement.

Fan and Wen [14] reported a model, in which evaporation and mobile condensates are considered. Li and Zhu [15] reported a new model that takes into account the condensation/evaporation and liquid diffusion by capillary actions, which is a function of fiber surface energy, contact angle and fabric pore size distributions. However in above Refs. [11–15], the models were based on the mass diffusion only due to the concentration gradient, the effect of the atmospheric pressure gradient on heat and moisture transfer in porous materials was ignored. In order to investigate the influence of atmospheric pressure gradient on heat and mass transfer within hygroscopic textile materials, and to provide insights on the functional design of clothing for windy conditions and active sportswear in outdoor, Li et al. [16] reported a new model by introducing new equations/terms and integrating them. They investigated the effect of atmospheric pressure on heat and moisture transfer.

All the above models did not consider the particle transfer processes in liquid water. For the transport in the porous media, Khilar and Fogler [17] originally proposed mathematical models describing the migration of fines in porous media are based on the release and capture mechanisms. For the pollutant transfer, Jiang and Corapcioglu [18] presented a hybrid equilibrium model of solute transport in porous media in the presence of colloids. But these models are established on the liquid water saturated porous media. The velocity of liquid water is assumed being constant. These assumptions may not be true in many situations. For instance, the heat and mass transfer in in vivo worn facemasks during breathing cycles, the liquid water is not saturated and the velocity is not a constant. The purpose of this paper is to report the development of a mathematical model to describe the complicated and coupled physical mechanisms, the numerical solution and validation of the model with experimental data.

2. Physical mechanisms of heat and mass transfer in the masks

We focus on the coupled processes of droplets contaminated with viruses transfer with other mass transfer in this paper. The liquid water contaminated with SARS viruses is propelled by surface tension force and breathing action. During the capillary action and breathing the water evaporation/condensation, sorption/desorption, virus deposition/release, and virus Brownian diffusion take place at the same time, as shown in Fig. 1.

We have made the following assumption: first, a local thermal equilibrium exists among all phases due to the small dimensions of the constituting fibers and the particles. Therefore, all phases have an identical temperature at a point in space. Second, swelling of the fibers due to changing moisture content is neglected. Third, the droplets transferred by capillary action, and the viruses in the droplets move and diffuse with the droplets

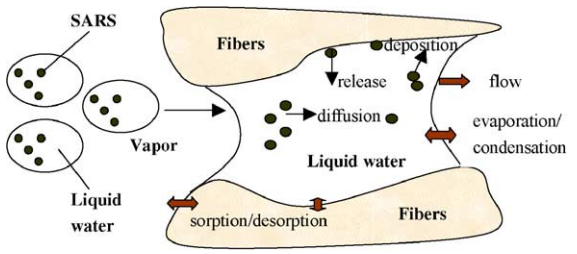

Fig. 1. The schematic map of SARS viruses transfer in the mask.

due to concentration gradient. The gas in void space between fibers includes: dry air, and water vapor. Fourth, the gas is assumed to satisfy the partial pressure law and the sate equation of the perfect gas. Fifth, the SARS viruses are sphere form with uniform size.

Let x denote the coordinate across the layer of the mask; $x = 0$ and $x = L$ indicate the positions at the inner and the outer surface of the mask. The t denotes time. According to the mass and energy balance laws, we can list the following balance equations: for water vapor:

$$\frac{\partial(\varepsilon_s C_a)}{\partial t} = \frac{\partial}{\partial x}\left[(D_M)\varepsilon_s \frac{\partial(C_a)}{\partial x}\right] - \frac{\partial(\varepsilon_s V_s C_a)}{\partial x} - \varpi_1 \varepsilon_f \frac{\partial C_f}{\partial t} + Q_1 \tag{1}$$

for whole gas:

$$\frac{\partial(\varepsilon_s C_s)}{\partial t} = -\frac{\partial(\varepsilon_s V_s C_s)}{\partial x} - \varpi_1 \varepsilon_f \frac{\partial C_f}{\partial t} + Q_1 \tag{2}$$

for liquid water:

$$\frac{\partial(\varepsilon_l \rho_l)}{\partial t} = -\frac{\partial(\varepsilon_l V_l \rho_l)}{\partial x} - \varpi_2 \varepsilon_f \frac{\partial C_f}{\partial t} - Q_1 \tag{3}$$

for virus in the liquid water:

$$\frac{\partial(\varepsilon_l C_v)}{\partial t} = \frac{\partial}{\partial x}\left[(D_B)\varepsilon_l \frac{\partial(C_v)}{\partial x}\right] - \frac{\partial(\varepsilon_l V_l C_v)}{\partial x} - \frac{\partial(\rho_v \varepsilon_v)}{\partial t} \tag{4}$$

for energy:

$$\begin{aligned}(c_v)_m \frac{\partial T}{\partial t} - \lambda_v \varepsilon_f \varpi_1 \frac{\partial C_f}{\partial t} - \lambda_l \varepsilon_f \varpi_2 \frac{\partial C_f}{\partial t} + \lambda(Q_1) \\ + [(C_a c_{p,a} + C_d c_{p,d})\varepsilon_s V_s + \rho_l c_l \varepsilon_l V_l] \frac{\partial T}{\partial x} \\ = \frac{\partial}{\partial x}\left(k_{mix} \frac{\partial T}{\partial x}\right)\end{aligned} \tag{5}$$

for deposition viruses on the fiber surface:

$$\frac{\partial(\rho_v \varepsilon_v)}{\partial t} = K_1 \varepsilon_l C_v - K_2 \rho_v \varepsilon_v \tag{6}$$

where ε_s is the volume fraction of gas, $\varepsilon_s = 1 - \varepsilon_f - \varepsilon_l - \varepsilon_v$, ε_f is the volume fraction of the fiber in the fabrics, ε_l is the volume of liquid water in a unit volume element, ε_v is the volume of virus in deposition on surface of fibers in a unit volume. C_a and C_v represent the concentration of water vapor in gas and virus concentration in liquid water respectively. C_s denotes the concentration of the whole gas. V_s and V_l are the intrinsical velocity of gas and liquid water respectively. ρ_l is the density of the liquid water. D_M is the molecular diffusion coefficient of the water vapor. $D_B = \frac{k_B T}{6\pi\mu_l r_v \tau}$ [19] is the Brownian diffusion coefficient of virus in liquid water, which is a function of temperature T, r_v is the radius of viruses and μ_l is the dynamic viscosity of liquid water, τ is correction coefficient for bend diffusion way and effect of non-continuity of liquid water droplets. k_B is the Boltzmann constant. ϖ_1 denotes the proportion of the sorption of water vapor by fibers, and ϖ_2 denotes the proportion of liquid water by fibers. Q_1 represents the evaporation rate of liquid water on the fibers. C_f is the water vapor concentration in the fiber. λ_v, λ_l, λ represent the sorption latent heat coefficients of the water vapor, liquid water and evaporation latent coefficient of liquid water respectively. $(c_v)_m$ is effective volume heat capacity, and k_{mix} is the effective thermal conductivity of fabric. In the present study, the dispersion phenomenon is treated as an additional diffusive term added to the stagnant component. The empirical equation employed by Amiri and Vafai [10] is employed as:

$$k_{mix} = \sum_{i=a,d,l,f} \varepsilon_i k_i + 0.5 \sum_{j=s,l} [P_r R_e]_j k_j \tag{7}$$

In Eq. (1), the term on the left side represents vapor storage within the void space of the inter-fiber, the first term on the right side represent the molecular diffusion of the water vapor, the second term represents the water vapor flow with the whole gas, the third term represents water vapor accumulation rate within the fiber, i.e. the sorption rate of fibers, whereas the fourth term is evaporation flux of the liquid water in the inter-fibers void space. The meanings of the terms in Eqs. (2)–(4) are similar as those in Eq. (1). Eq. (5) represents the energy balance. The first term on the left side of Eq. (5) represents energy storage, the second and third term represent sorption latent heat of water vapor by fibers and the latent heat of liquid water within inter-fibers respectively; the fourth term represents the latent heat of evaporation of liquid water, and the fifth term represents the convective heat transfer. The right side represents the heat conduct ion. When the viruses are stable, in other words, when they do not deposit on collector (matrix) surfaces, they can migrate in the liquid water. However, when they are unstable, they can deposit and attach to solid surface. Both types of phenomenon can be observed simultaneously. The first-order rate Eq. (6) provides the kinetic expression for simultaneous virus capture/release mechanisms. The deposition rate coefficient K_1 can be calculated by making use of the collector approach.

Gruesbeck and Collins [20] proposed a two-parameters rate expression for spherical collectors. Here, we consider the fibrous collectors and give below [20]:

$$K_1 = (c_e S_v E + b\varepsilon_v)V_l \tag{8}$$

where c_e is effective capture area coefficient of the collectors, S_v is the specific area of fabrics, E is the retention efficiency, b is the adjustable parameter. The second term gives the additional capture of viruses due to bridging, which increases with the amount of viruses deposited. The release coefficient K_2 is a function of velocity of liquid water [20]:

$$K_2 = \begin{cases} c_r(V_l - V_c)\varepsilon_l & V_l > V_c \\ 0 & V_l \leqslant V_c \end{cases} \tag{9}$$

where c_r is the release coefficient of the virus, V_c is the critical velocity.

Evaporation rate of liquid water on the fibers can express as following [15]:

$$Q_l = \varepsilon_s h_{l\leftrightarrow g} S_v (C_a^*(T) - C_a) \tag{10}$$

where S_v denotes the specific volume of fabric. $C_a^*(T)$ is the saturated water vapor concentration and solely determined by the temperature.

Sorption and desorption of moisture by the fibers obey the Fickian law [12]:

$$\frac{\partial C_f(x,r,t)}{\partial t} = \frac{1}{r}\frac{\partial}{\partial r}\left[rD_f(x,t)\frac{\partial C_f(x,r,t)}{\partial r}\right] \tag{11}$$

where $D_f(x,t)$ is the diffusion coefficient of water vapor in the fiber, r is the radial coordinate in a fiber. The boundary condition is determined by the relative humidity of the air surrounding a fiber at x.

It is known that in flow through a porous medium the pressure drop caused by frictional drag is directly proportional to velocity for low speed flow. At higher velocities, inertial effects become appreciable, causing an increase in the form drag. As Vafai and Tien [9] pointed that the pressure drop in the bulk of porous medium is proportional to a linear combination of flow velocity and square of the flow velocity. The square term is caused by the inertial effects offered through the solid matrix, it is a function of Reynolds number and geometry of porous media. In the present case, the gas velocity during normal breathing cycles is small and the pore size of mask N95 and fiber radius are small, so the Reynolds number is small (Re_{max} is about 3). Therefore, the inertial effects can be ignored. Therefore, we can assume the relationship of pressure drop and velocity satisfies the Darcy's law:

$$\varepsilon_s V_s = -\frac{KK_{rs}}{\mu_s}\frac{\partial p_s}{\partial x} \tag{12}$$

$$\varepsilon_l V_l = -\frac{KK_{rl}}{\mu_l}\left(\frac{\partial p_s}{\partial x} - \frac{\partial p_c}{\partial x}\right) \tag{13}$$

where p_s is the pressure of gas. p_c is capillary pressure. μ_s and μ_l are the dynamic viscosity of gas and liquid water respectively. Extending the results of Ref. [15], we can obtain:

$$K = \frac{3\varepsilon \sin^2\beta d_c^2}{80} \tag{14}$$

where K is the intrinsical permeability, β is the average angle of the capillaries in the material, d_c is effective radius of the pores in material, ε is the porosity of material. The relative permeability of liquid water [15]:

$$K_{rl} = (\varepsilon_l/\varepsilon)^3 \tag{15}$$

The relative permeability of the gas [21]:

$$K_{rs} = 1 - K_{rl} \tag{16}$$

The relation of capillary pressure p_c and the volume fraction of liquid water ε_l [15]:

$$\frac{\partial p_c}{\partial x} = -\frac{2\sigma\cos\phi\varepsilon}{\varepsilon_l^2 d_c}\frac{\partial \varepsilon_l}{\partial x} \tag{17}$$

where σ is the surface tension and ϕ is the contact angle.

According to the basic assumption of the perfect gas, we have:

$$C_s = \frac{M_s p_s}{RT} \tag{18}$$

Then,

$$\frac{\partial(\varepsilon_s C_s)}{\partial t} = \frac{M_s\varepsilon_s}{RT}\frac{\partial(p_s)}{\partial t} - p_s\frac{\varepsilon_s M_s}{RT^2}\frac{\partial T}{\partial t} - \frac{M_s p_s}{RT}\frac{\partial \varepsilon_l}{\partial t} - \frac{M_s p_s}{RT}\frac{\partial \varepsilon_v}{\partial t} \tag{19}$$

Substitution of Eqs. (8)–(19) into Eqs. (1)–(6) yields:

$$\varepsilon_s\frac{\partial(C_a)}{\partial t} - C_a\frac{\partial(\varepsilon_l)}{\partial t} = \frac{\partial}{\partial x}\left[D\frac{\partial(C_a)}{\partial x}\right] + \frac{\partial}{\partial x}\left[G\frac{\partial p_s}{\partial x}\right] - C + Q_l + C_a\frac{\partial(\varepsilon_v)}{\partial t} \tag{20}$$

$$A_3\frac{\partial(p_s)}{\partial t} + A_4\frac{\partial T}{\partial t} + A_5\frac{\partial \varepsilon_l}{\partial t} = \frac{\partial}{\partial x}\left[GS\frac{\partial p_s}{\partial x}\right] - C + Q_l - A_5\frac{\partial \varepsilon_v}{\partial t} \tag{21}$$

$$\rho_l\frac{\partial(\varepsilon_l)}{\partial t} = \frac{\partial}{\partial x}\left[GL\frac{\partial p_s}{\partial x}\right] + \frac{\partial}{\partial x}\left[(DL)\frac{\partial \varepsilon_l}{\partial x}\right] - C_l - Q_l \tag{22}$$

$$\varepsilon_l\frac{\partial(C_v)}{\partial t} + C_v\frac{\partial(\varepsilon_l)}{\partial t} = \frac{\partial}{\partial x}\left[DV\frac{\partial(C_v)}{\partial x}\right] + \frac{\partial}{\partial x}\left[GV\frac{\partial p_s}{\partial x}\right] + \frac{\partial}{\partial x}\left((DLV)\frac{\partial \varepsilon_l}{\partial x}\right) - \frac{\partial(\rho_v\varepsilon_v)}{\partial t} \tag{23}$$

$$(c_v)_m\frac{\partial T}{\partial t} - \lambda_v C - \lambda_l C_l + \lambda(Q_l) + [(C_a c_{p,a} + C_d c_{p,d})\varepsilon_s V_s + \rho_l c_l \varepsilon_l V_l]\frac{\partial T}{\partial x} = \frac{\partial}{\partial x}\left(k_{mix}\frac{\partial T}{\partial x}\right) \tag{24}$$

$$\frac{\partial(\varepsilon_v)}{\partial t} = \frac{1}{\rho_v}K_1\varepsilon_l C_v - K_2\varepsilon_v \tag{25}$$

where $\varepsilon_s = 1-\varepsilon_f-\varepsilon_l-\varepsilon_v$, $D = DM\varepsilon_s$, $\varepsilon = \varepsilon_0-\varepsilon_v$,

$G = C_a\frac{3\varepsilon\sin^2\beta d_c^2}{80\mu_s}\left(1-\left(\frac{\varepsilon_l}{\varepsilon}\right)^3\right)$,

$C = \varpi_1(1-\varepsilon)\dfrac{\partial C_f}{\partial t}$, $A_3 = \dfrac{M_s(1-\varepsilon_f-\varepsilon_l-\varepsilon_v)}{RT}$,

$A_4 = -p_s\dfrac{(1-\varepsilon_f-\varepsilon_l-\varepsilon_v)M_s}{RT^2}$

$GS = \dfrac{M_s p_s}{RT}\dfrac{3\varepsilon\sin^2\beta d_c^2}{80\mu_s}\left(1-\left(\dfrac{\varepsilon_l}{\varepsilon}\right)^3\right)$, $A_5 = -\dfrac{M_s p_s}{RT}$,

$GL = \rho_l\dfrac{3\varepsilon\sin^2\beta d_c^2}{80\mu_l}\left(\dfrac{\varepsilon_l}{\varepsilon}\right)^3$

$DL = \rho_l\dfrac{3\sin^2\beta d_c\sigma\cos\phi\varepsilon_l}{40\varepsilon\mu_l}$, $C_1 = \varpi_2(1-\varepsilon)\dfrac{\partial C_f}{\partial t}$,

$DV = (D_B)\varepsilon_l$

$GV = C_v\dfrac{3\sin^2\beta d_c^2}{80\varepsilon^2\mu_l}\varepsilon_l^3$, $DLV = C_v\dfrac{3\sin^2\beta d_c\sigma\cos\phi\varepsilon_l}{40\varepsilon\mu_l}$

2.1. Initial and boundary conditions

In order to generate a solution to above mentioned equations, we need to specify an initial condition and boundary conditions at the mask surfaces in terms of humidity, temperature, vapor content, liquid water content, the concentration of virus in the liquid water and temperature respectively. Fig. 2 is a schematic diagram to show the initial and boundary conditions of facemask. Initially, a mask is equilibrated to a given atmosphere of temperature and humidity, the temperature, moisture content and virus concentration are uniform throughout the mask at known values.

$$\begin{aligned} &T(x,0) = T_0\\ &C_v(x,0) = C_{v0}\\ &\varepsilon_l(x,0) = \varepsilon_{l0}\\ &p_s(x,0) = p_{s0}\\ &C_f(x,0) = f(RH_0,T_0)\\ &C_a(x,0) = C_{a0} \end{aligned} \tag{26}$$

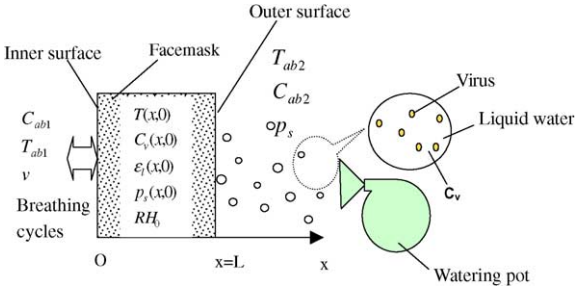

Fig. 2. Schematic diagram of initial and boundary conditions of facemask.

Then, the boundaries of the mask are exposed to two different environments:

For simulation the breathing process, at $x = 0$ (the mask inner surface), we have

$$\begin{aligned} &\left(D\frac{\partial(C_a)}{\partial x}+G\frac{\partial p_s}{\partial x}\right)\Big|_{x=0} = -\varepsilon_s\kappa(C_{ab1}v)\\ &\left(GS\frac{\partial p_s}{\partial x}\right)\Big|_{x=0} = -\varepsilon_s\kappa(C_{sb1}v)\\ &\left(GL\frac{\partial p_s}{\partial x}+(DL)\frac{\partial\varepsilon_l}{\partial x}\right)\Big|_{x=0} = -h_{l\leftrightarrow g}\varepsilon_l(C_a^*(T)-C_{ab1})\\ &\left(DV\frac{\partial(C_v)}{\partial x}+GV\frac{\partial p_s}{\partial x}+(DLV)\frac{\partial\varepsilon_l}{\partial x}\right)\Big|_{x=0} = 0\\ &k_{mix}\frac{\partial T}{\partial x}\Big|_{x=0} = -h_{t1}(T-T_{ab1})-\lambda h_{l\leftrightarrow g}\varepsilon_l(C_a^*(T)-C_{ab1}) \end{aligned} \tag{27}$$

where v is the velocity of the breathing out. $v = v_0\sin(\frac{\pi}{2}t)$, v_0 is the peak value of breathing velocity. κ is the ratio of area of nares to effective ventilation area of the mask. C_{ab1}, C_{sb1} denote the concentration of water vapor and whole gas. If person breath out C_{ab1}, C_{sb1} are ambient values, else they are taken values on position $x = 0$. h_{t1} is the combined heat exchange coefficient. It is the sum of radiation heat exchange coefficient and convective heat exchange coefficient, which is a function of the flow velocity.

At $x = L$ (the mask outer surface), we have the following boundary conditions to take into account the convective of the boundary air layer:

$$\begin{aligned} &\left(D\frac{\partial(C_a)}{\partial x}+G\frac{\partial p_s}{\partial x}\right)\Big|_{x=L} = -h_c\varepsilon_s(C_a-C_{ab2})\\ &k_{mix}\frac{\partial T}{\partial x}\Big|_{x=L} = -h_{t2}(T-T_{ab2})-\lambda h_{l\leftrightarrow g}\varepsilon_l(C_a^*(T)-C_{ab2})\\ &\left(GL\frac{\partial p_s}{\partial x}+(DL)\frac{\partial\varepsilon_l}{\partial x}\right)\Big|_{x=L} = -h_{l\leftrightarrow g}\varepsilon_l(C_a^*(T)-C_{ab2})\\ &p_s(L,t) = p_{sb2}\\ &\left(DV\frac{\partial(C_v)}{\partial x}+GV\frac{\partial p_s}{\partial x}+(DLV)\frac{\partial\varepsilon_l}{\partial x}\right)\Big|_{x=L} = 0 \end{aligned} \tag{28}$$

where h_c is the convection mass transfer coefficient, h_{t2} is the combined heat exchange coefficient.

3. Numerical method of the model

To derive a numerical solution for Eqs. (20)–(28) by using the finite volume method, we select a control volume, as shown in Fig. 3.

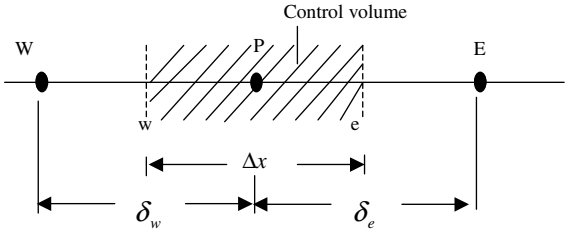

Fig. 3. Schematic map of control volume.

For example, a simplified integral form is used for Eq. (20) in a control volume P.

$$\int_{\Omega_P}\left(\varepsilon_s\frac{\partial(C_a)}{\partial t}-C_a\frac{\partial(\varepsilon_l)}{\partial t}-C_a\frac{\partial(\varepsilon_v)}{\partial t}+C-Q_1\right)dx = \int_{\Omega_P}\left(\frac{\partial}{\partial x}\left[D\frac{\partial(C_a)}{\partial x}\right]+\frac{\partial}{\partial x}\left[G\frac{\partial p_s}{\partial x}\right]\right)dx \quad (29)$$

Then,

$$\frac{(\varepsilon_s)_P^n[(C_a)_P^{n+1}-(C_a)_P^n]}{\Delta t}\Delta x-\frac{(C_a)_P^n[(\varepsilon_l)_P^{n+1}-(\varepsilon_l)_P^n]}{\Delta t}\Delta x + C_P^n\Delta x-Q_{1P}^n\Delta x-\left[C_a\frac{\partial(\varepsilon_v)}{\partial t}\right]_P^n\Delta x = \left[D\frac{\partial(C_a)}{\partial x}\right]_e-\left[D\frac{\partial(C_a)}{\partial x}\right]_w+\left[G\frac{\partial p_s}{\partial x}\right]_e-\left[G\frac{\partial p_s}{\partial x}\right]_w \quad (30)$$

The right terms of Eq. (30) can write as following:

$$\left[D\frac{\partial(C_a)}{\partial x}\right]_e-\left[D\frac{\partial(C_a)}{\partial x}\right]_w+\left[G\frac{\partial p_s}{\partial x}\right]_e-\left[G\frac{\partial p_s}{\partial x}\right]_w = D_e^n\frac{(C_a)_e^{n+1}-(C_a)_P^{n+1}}{\delta_e}-D_w^n\frac{(C_a)_P^{n+1}-(C_a)_W^{n+1}}{\delta_w} + G_e^n\frac{(p_s)_e^{n+1}-(p_s)_P^{n+1}}{\delta_e}-G_w^n\frac{(p_s)_P^{n+1}-(p_s)_W^{n+1}}{\delta_w} \quad (31)$$

Substitution of Eq. (31) into Eq. (30) yields:

$$K_1(C_a)_W^{n+1}+K_2(p_s)_W^{n+1}+K_3(C_a)_P^{n+1}+K_4(p_s)_P^{n+1} + K_5(C_a)_e^{n+1}+K_6(p_s)_e^{n+1}+K_7(\varepsilon_l)_P^{n+1}=R_1 \quad (32)$$

Let $\mu_w=\frac{\Delta t}{\Delta x\delta_w}$, $\mu_e=\frac{\Delta t}{\Delta x\delta_e}$ where

$$K_1=\mu_wD_w^n,\quad K_2=\mu_wG_w^n,$$
$$K_3=-(\mu_wD_w^n+\mu_eD_e^n+(\varepsilon_s)_P^n),$$
$$K_4=-(\mu_wG_w^n+\mu_eG_e^n),\quad K_5=\mu_eD_e^n,$$
$$K_6=\mu_eG_e^n,\quad K_7=(C_a)_P^n$$

$$R_1=-(\varepsilon_sC_a)_P^n+(\varepsilon_lC_a)_P^n+C_P^n\Delta t-Q_{1P}^n\Delta t-\left[C_a\frac{\partial(\varepsilon_v)}{\partial t}\right]_P^n\Delta t$$

At $x=L$,

$$\left[D_{N-1/2}^n\frac{(C_a)_N^{n+1}-(C_a)_{N-1}^{n+1}}{\delta_{Nw}}\right]+\left[G_{N-1/2}^n\frac{(p_s)_N^{n+1}-(p_s)_{N-1}^{n+1}}{\delta_{Nw}}\right] = -h_c(\varepsilon_s)_N^n(C_{aN}^{n+1}-C_{ab2}) \quad (33)$$

At $x=0$,

$$\left[D_{1+1/2}^n\frac{(C_a)_2^{n+1}-(C_a)_1^{n+1}}{\delta_{1e}}\right]+\left[G_{1+1/2}^n\frac{(p_s)_2^{n+1}-(p_s)_1^{n+1}}{\delta_{1e}}\right] = -(\varepsilon_s)_N^n\kappa(C_{ab}v) \quad (34)$$

Following the same procedure as for the water vapor mass conservation, we can derive the discretization equations for liquid water, energy, whole gas and virus. By specifying initial conditions we can calculate the coefficient of the discretization and its right term, the values of water vapor concentration, liquid water fraction, temperature and atmospheric pressure and concentration of virus at next time can be obtained.

4. Numerical solutions and discussion

4.1. Experimental validation and simulation

In order to investigate the prediction ability of the present model, we compare the predictions from the model with the experimental observations reported else by Li et al. [23]. Briefly, an in vivo wear filtration efficiency trial was carried by using human subjects. In the trial, each subject was asked to put on a N95 facemask and started to perform walking exercise. The researcher sprayed the simulated viral solution onto the facemask once at a distance 1 m every 10 min. The simulated viral solution was sprayed on the mask seven times during the walking in total. The average weight of the splash in one stroke of spray was 2 ml. The simulated viral solution was made up with KCl (potassium chloride) water solution, in which the K^+ concentration is 0.02 g/cm^3. Seventy minutes later K^+ content of each layer was obtained. Further, the relative K^+ content of each layer to K^+ content of the whole mask was calculated by dividing the K^+ content of each layer with the sum of K^+ content of all layers for each mask. All the percentages were used as the basis for analysis of the test results for four layers of N95 masks. The initial and boundary's conditions in simulation are listed in Table 1. The computation parameters are listed in Table 2.

Table 1
The initial and boundary's conditions in simulation

Initial condition	Boundary's conditions at the mask inner surface ($x = 0$)	Boundary's conditions at the mask outer surface ($x = L$)
$T(x,0) = 25\,^{\circ}\mathrm{C}$ $C_v(x,0) = (1.0\mathrm{e}{-10})\%$ $\varepsilon_l(x,0) = 1.0\mathrm{e}{-3}$ $p_s(x,0) = 1.01325\mathrm{e}5$ Pa $RH_0 = 65\%$	In Eq. (27): $C_{ab1}(0,t) = C^*_a(T_{ab1})$ $T_{ab1} = 37\,^{\circ}\mathrm{C}$ $v_0 = 0.2$ m/s	In Eq. (28): $T_{ab2} = 25\,^{\circ}\mathrm{C}$ $C_{ab2} = C^*_a(T_{ab2}) \times 65\%$ $p_s(L,t) = 1.01325\mathrm{e}5$ Pa Additional conditions: If $t = 0, 600, 1200, \ldots, 3600$ s Change: $C_v(L,t) = [0.02 \times 10^3 \times 0.5 + \varepsilon_l(L, t-\Delta t) \times C_v(L, t-\Delta t)]/0.5$ $\varepsilon_l(L,t) = 0.5$

Table 2
The computation parameters

Parameters	Symbol	Unit	Value and reference
Density of a fiber	ρ_f	kg/m^3	910 [12]
Volumetric heat capacity of fabric	C_{vf}	kJ/m^3 K	1715 [12]
Thermal conductivity of fabric	k_{fab}	W/m^2 K	5.18e–2 [12]
Heat of sorption of water vapor by fibers	λ	kJ/kg	2522 [15]
Heat of sorption or desorption of liquid water by fibers	λ_l	kJ/kg	2522 [15]
Heat of sorption or desorption of water vapor by fibers	λ_v	kJ/kg	2260 [15]
Convection mass transfer coefficient	h_{c2}	m/s	1.37e–2
Mass transfer coefficient	$h_{l\leftrightarrow g}$	m/s	1.37e–2
Combined heat transfer coefficient	h_t	W/m^2 K	81.6
Diffusion coefficient of water vapor in fiber	$D_f(w_c, t)$	m^2/s	1.3e–13 [15]
Dynamic viscosity of gas	μ_s	kg/m s	1.83e–5 [22]
Dynamic viscosity of liquid water	μ_l	kg/m s	1.0e–3 [22]
Contact angle	ϕ	°C	80
Effective radius of pore in fabrics	d_c	m	5.0e–7
Surface tension	σ	N/m	31
Average angle of the capillaries in fabrics	β	°C	20
Molecular diffusion coefficient	D_a	m^2/s	2.5e–5
Thickness of N95 mask	L_{N95}	m	5.1e–3
Special surface	S_v	1/m	10000
Effective capture area coefficient of the collectors	c_e	–	0.1
Retention efficiency	E	–	0.01
Critical velocity	V_c	m/s	1.0e–7
Release coefficient of the virus	c_r	–	0.3

We simulated above progress and the comparisons of the simulation and the experimental results of the N95 mask in the relative K^+ content in each layer are shown in Fig. 4.

As Fig. 4 shows, the layer 1 (the outer layer of the masks) has the highest K^+ contents, as they were exposed to the simulated viral loading, followed by the second layer and third layer, as well as the fourth layer of N95 masks. We can also see that the simulated relative K^+ content of the outer layer is slightly lower than the experiment data, and a little higher in the second layer. It is because that the effect of layer gap is not considered. However, it can be seen that the trend predicted by the model agrees well with that of the experiment.

Using above condition, we can also obtain the transfer progresses of the K^+ concentration, liquid water, water vapor concentration, pressure and temperature during breathing cycles.

Fig. 5 shows the distribution of the K^+ concentration in liquid water variation in the fabric with the time. The K^+ concentration in liquid water of outer layer ($x = L$) decreases after every splash and increases with the evaporation of liquid water and then decreases again due to the K^+ diffusion from high to low concentration areas.

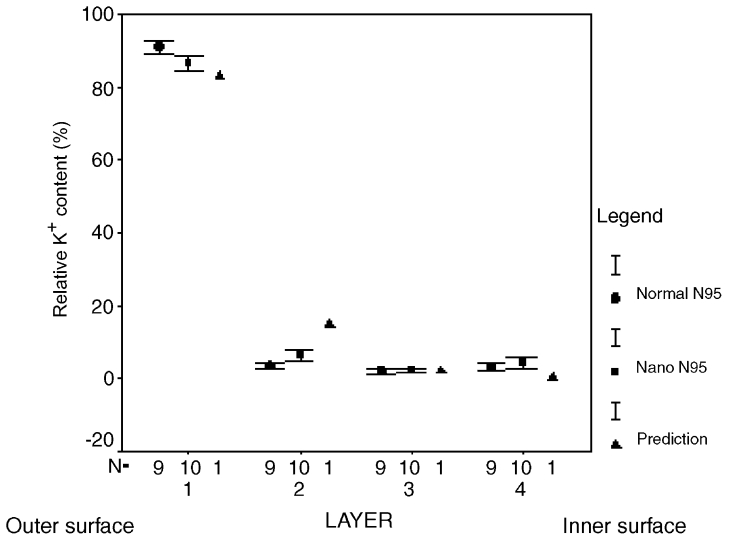

Fig. 4. Comparison of measured relative K^+ content with predictions from the model.

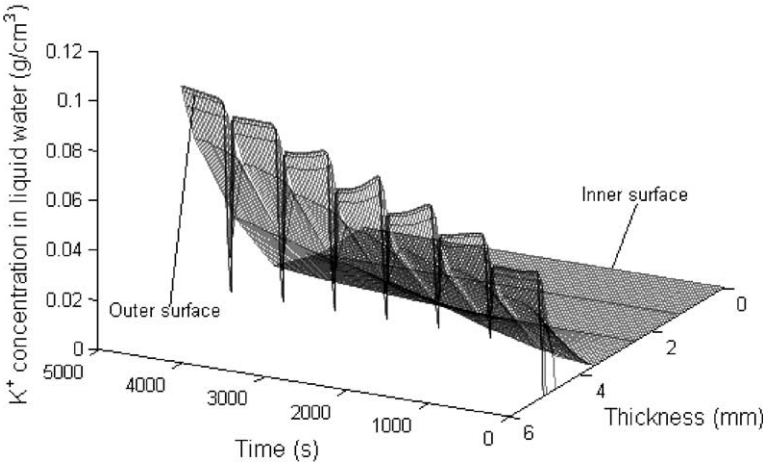

Fig. 5. Distribution of the K^+ concentration in liquid water.

The fraction of deposition K^+ on the surface of fibers is shown in Fig. 6. The fraction of deposition K^+ on the surface of fibers of the outer surface increases gradually with the progress of splash on the outer surface. But K^+ deposits very little in the deeper layers as the liquid water does not diffuse into the mask very far.

From Fig. 7 we can see the distribution of the liquid water in the mask with the time in 600 s, which is enlarged to show the dynamic transfer processes. We can see the variation progress of the liquid water fraction by the capillary pressure and evaporation. Since the contact angle is large and the effective radius of the capillary is small, the diffusion velocity of the liquid water is slow. The liquid water of outer surface evaporates quickly since the relative humidity of the environment is slow. Liquid water appears on the inner surface due to the condensation from high humidity of air breathed out.

Fig. 8 shows the K^+ content in the liquid water. We can see the K^+ content on outer surface is the highest at the beginning of the splash, gradually diffuses in wards.

Fig. 9 shows the distribution of atmospheric pressure during breathing. The pressure increases quickly in the process of breathing out because the effect of resistance of the mask to air flow and opposite trend can be seen during the process of breathing in. The pressure changes periodically with the breathing cycles.

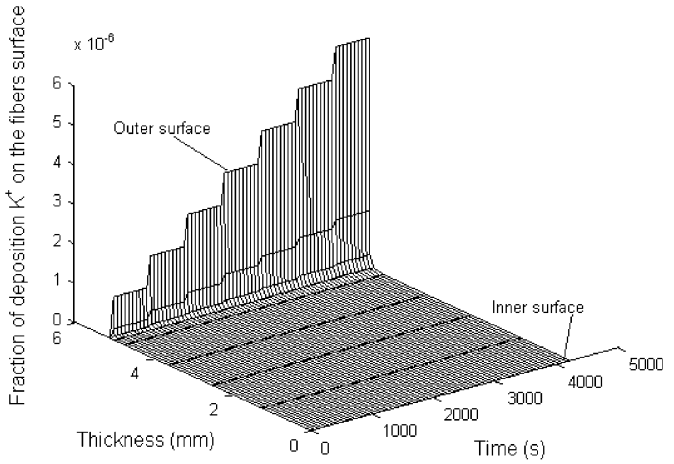

Fig. 6. Distribution of the fraction of deposition K^+ on the fibers surface.

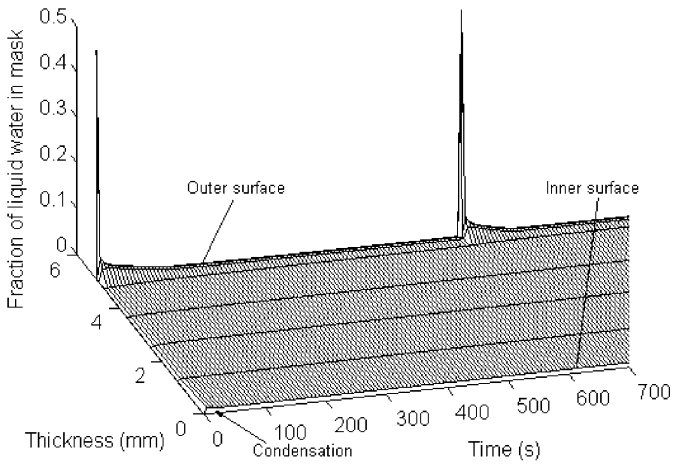

Fig. 7. Distribution of the liquid water.

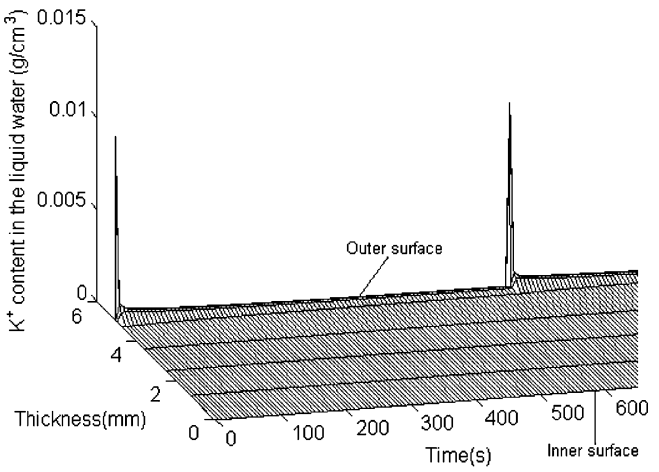

Fig. 8. K^+ content in the liquid water.

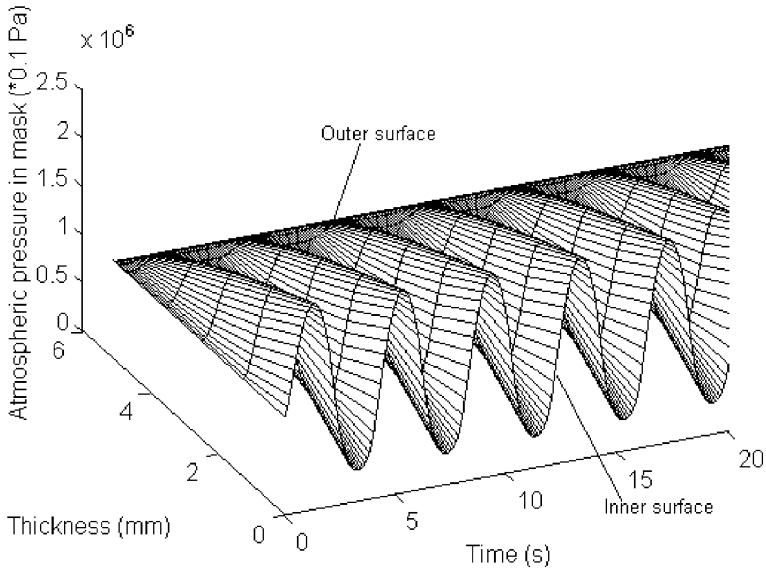

Fig. 9. Distribution of atmospheric pressure.

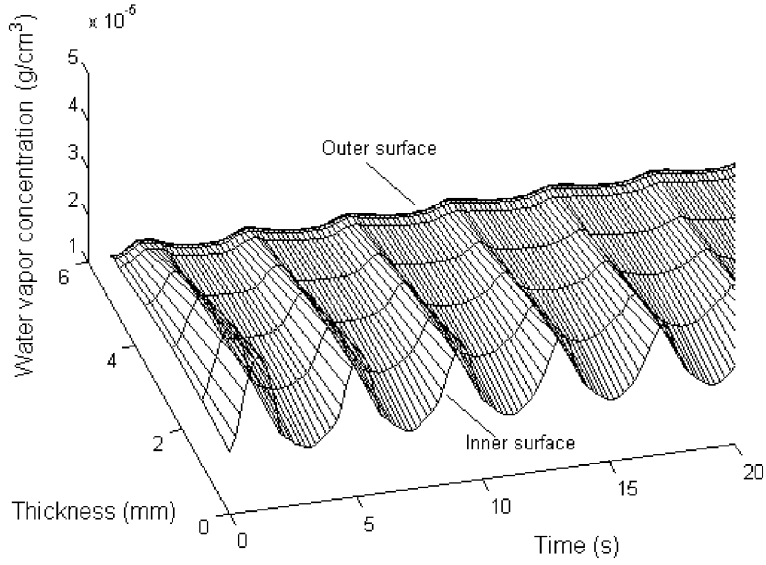

Fig. 10. Distribution of water vapor concentration.

As shown in Fig. 10, the concentration of water vapor varies periodically with the breathing cycles. When a person breathes out the air, the water vapor concentration increases, and then, the water vapor concentration decreases during the breathing in process.

Fig. 11 shows the temperature distribution. The temperature change is controlled by convective heat transfer and the evaporation/condensation of water. The temperature on the inner surface increases gradually, as the body temperature is higher than that of mask. The temperature on the outer surface decreases as the liquid water evaporates and heat is adsorbed. Meanwhile, the temperature changes periodically with the breathing cycles. When a person breathes out the air, the water vapor concentration on the surface of the fibers is increased and the relative humidity of air is increase, so that water vapor condenses and releases the latent heat. Also, the air convective heat transfer occurs during breathing cycles. When the person breathes in the air, the opposite occurs.

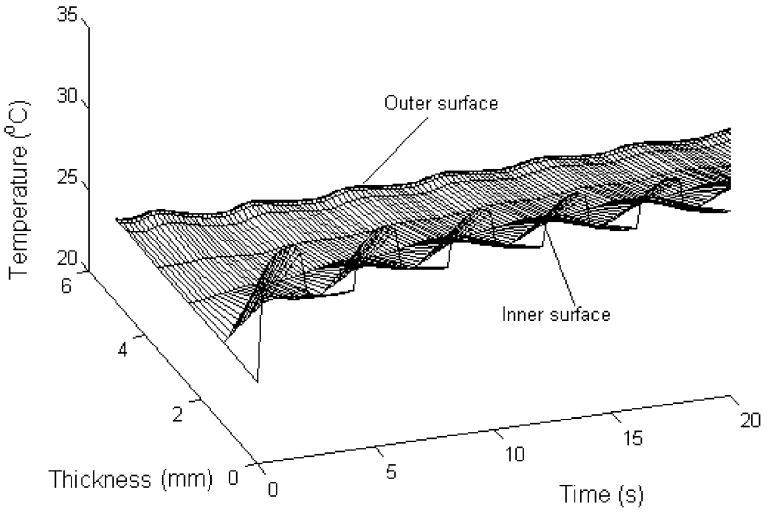

Fig. 11. Temperature distribution.

4.2. Effects of the structures and materials properties on virus content

In order to investigate the effects of structures and materials properties on virus content(i.e. $\varepsilon_l \times C_v$) transferred to the mask inner surface, we simulate masks with different effective capillary radius, thickness and contact angle and compare the simulation results. The simulation conditions are the same described in Section 4.1.

Fig. 12 shows the effect of the effective capillary radius on virus content on the facemask inner surface. The larger effective capillary is, the more viruses are deposited on the facemask inner surface becomes.

Fig. 13 shows the effect of the thickness of facemask on virus content on the inner surface. The virus content on the inner surface of mask with small thickness is more than that with large thickness.

Fig. 14 shows the effect of the contact angle on virus content on the facemask inner surface. The larger contact angle is, the smaller amount of viruses on the spread to facemask inner surface during breathing cycles.

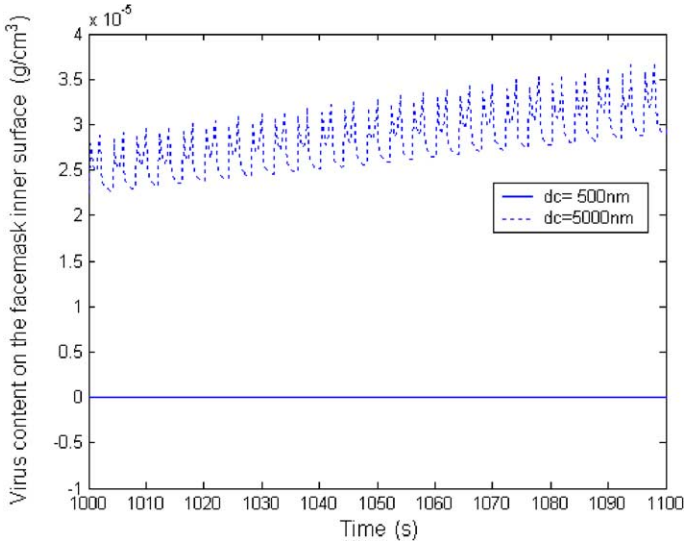

Fig. 12. Effect of the effective capillary radius on virus content on the facemask inner surface.

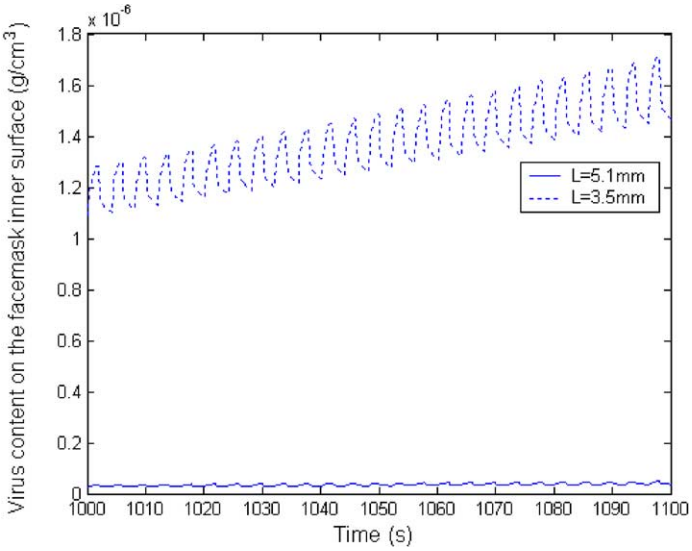

Fig. 13. Effect of the thickness on virus content on the facemask inner surface.

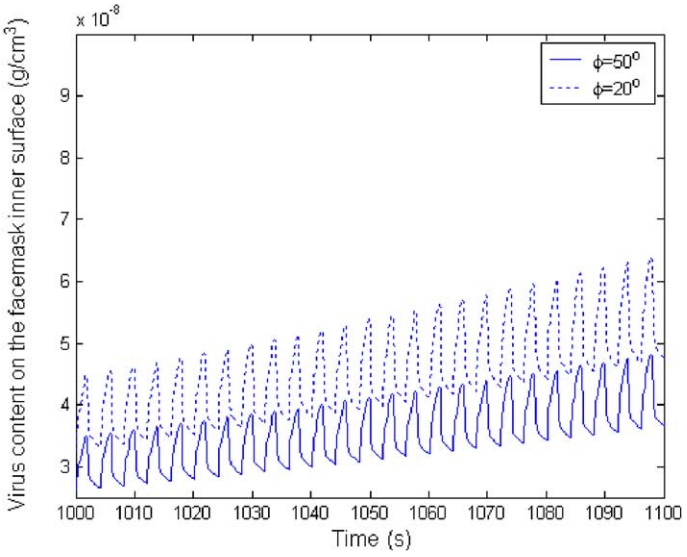

Fig. 14. Effect of the contact angle on virus content on the facemask inner surface.

5. Conclusion

In order to provide the critical theoretical analysis on mask thermal and moisture comfort and protective performance during wear, we report the development of a coupled heat and mass transfer model to describe the virus diffusion in the mask during breathing cycles. From the simulation, we can conclude that:

1. The predictions given by the model agree well with that of the experiment, indicating that the model has good prediction ability.
2. For material with large contact angle and small pore size such as N95 mask, the effect of breathing cycles on liquid water diffusion is small, but that on water vapor concentration and gas pressure is large. The viruses transfer in the mask mainly by diffusion in liquid water, and the evaporation of liquid water increases the virus concentration in liquid water. The virus mass in liquid water is larger than that on the surface of fibers in deposition because of small penetration velocity of liquid water.
3. The concentration of water vapor and pressure of the gas in the mask change periodically with the

breathing cycles. The temperature of mask also changes periodically with the breathing cycles.

4. Decrease the effective capillary radius, increase the thickness and contact angle can restrain the virus transfer from outer surface to inner surface of the facemask.

Acknowledgement

The authors wish to express their appreciation to Mr. Guan Yingting, Ms. Yao Lei and Mr. Ying Boan for their helpful discussions and to the Hong Kong Polytechnic University for funding this research through the projects A188 and GU027.

References

[1] We have been warned, Nature 424 (6945) (2003) 113.
[2] S.K. Chen, V.D. Brosseau, Evaluation of single-use masks and respirators for protection of healthcare workers against mycobacterial aerosols, Am. J. Infect. Contr. 22 (2) (1994) 65–74.
[3] K. Willkem, Y. Qian, J. Donnelly, et al., Penetration of airborne microorganisms through a surgical mask and a dusk/mist respirator, Am. Indust. Hygie. Assoc. J. 57 (4) (1996) 348–355.
[4] Y. Qian, K. Willkem, S.A. Grinshpun, et al., Performance of N95 respirators: Filtration efficiency for airborne microbial and inert particles, Am. Indust. Hygie. Assoc. J. 59 (2) (1998) 128–132.
[5] Y. Ogniewicz, C.L. Tien, Analysis of condensation in porous insulation, Int. J. Heat Mass Transfer 24 (3) (1981) 421–429.
[6] S. Motakef, M.A. El-Masri, Simultaneous heat and mass transfer with phase change in a porous slab, Int. J. Heat Mass Transfer 29 (10) (1986) 1503–1512.
[7] A.P. Shapiro, S. Motakef, Unsteady heat and mass transfer with phase change in porous slab: analytical solutions and experimental results, Int. J. Heat Mass Transfer 33 (1) (1990) 163–173.
[8] A. Bouddour, J.-L. Auriault, M.M.-A.J.-F. Bloch, Heat and mass transfer in wet porous media in presence of evaporation/condensation, Int. J. Heat Mass Transfer 41 (15) (1998) 2263–2277.
[9] K. Vafai, C.L. Tien, Boundary and inertia effects on flow and heat transfer in porous media, Int. J. Heat Mass Transfer 24 (2) (1981) 195–203.
[10] A. Amiri, K. Vafai, Analysis of dispersion effects and non-thermal equilibrium non-Darcian, variable porosity incompressible flow through porous medium, Int. J. Heat Mass Transfer 37 (6) (1994) 939–954.
[11] Y. Li, B.V. Holcombe, A two-stage sorption model of the coupled diffusion of moisture and heat in wool fabric, Textile Res. J. 62 (4) (1992) 211–217.
[12] Y. Li, Z.X. Luo, Physical mechanisms of moisture diffusion into hygroscopic fabrics during humidity transients, J. Textile Inst. 91 (2) (2000) 302–323.
[13] Z.X. Luo, J.T. Fan, Y. Li, Heat and moisture transfer with sorption and condensation in porous clothing assemblies and numerical simulation, Int. J. Heat Mass Transfer 43 (16) (2000) 2989–3000.
[14] J.T. Fan, X.H. Wen, Modeling heat and moisture transfer through fibrous insulation with phase change and mobile condensates, Int. J. Heat Mass Transfer 45 (19) (2002) 4045–4055.
[15] Y. Li, Q.Y. Zhu, A model of coupled liquid moisture and heat transfer in porous textiles with consideration of gravity, Num. Heat Transfer Part A 43 (5) (2003) 501–523.
[16] F.Z. Li, Y. Li, Y.X. Liu, et al., Numerical simulation of coupled heat and mass transfer in hygroscopic porous materials considering the influence of atmospheric pressure, Num. Heat Transfer Part B 45 (3) (2004) 249–262.
[17] K.C. Khilar, H.S. Fogler, Water sensitivity of sandstones, Soc. Pet. Engine J. 23 (1) (1983) 55–64.
[18] S.Y. Jiang, M.Y. Corapcioglu, A hybrid equilibrium model of solute transport in porous media in the presence of colloids, Coll. Surf. A: Physicochem. Eng. Aspects 73 (1993) 275–286.
[19] P. Lançon, G. Batrouni, L. Lobry, et al., Brownian walker in a confined geometry leading to a space-dependent diffusion coefficient, Physica A 304 (1) (2002) 65–76.
[20] C. Gruesbeck, R.E. Collins, Entrainment and deposition of fine particles in porous media, Soc. Pet. Engine J. 22 (1982) 847–856.
[21] S.B. Nasrallah, P. Perre, Detailed study of a model of heat and mass transfer during convective drying of porous media, Int. J. Heat Mass Transfer 31 (5) (1988) 957–967.
[22] S.M. Yang, Heat Transfer, second ed., Higher Educational Press, Beijing, 1980 (in Chinese).
[23] Y. Li, J. Chung, T. Wong, et al., In-vivo Protective Performance of Facemasks Coated with Nano Functional Materials, Hong Kong SARS Forum and Hospital Authority Convention, Hong Kong, 2004, p. 118.